Vibration and Tracking Control of Industrial Robots: A Comparison between Time-Varying Filtered B-Splines and Input Shaping

Iago Alves Pereira Department of Mechanical Engineering Department of Mechanical Engineering Department of Mechanical Engineering University of Michigan Ann Arbor, USA ipereira@umich.edu

Nosakhare Edoimioya University of Michigan Ann Arbor, USA nosed@umich.edu

Chinedum E. Okwudire University of Michigan Ann Arbor, USA okwudire@umich.edu

Abstract—The structural flexibility of industrial robot arms makes them vibrate when they are commanded to move at fast operation speeds. Among the control strategies, feedforward control stands out as an interesting approach to suppress vibration since it does not create stability issues and works for repeating and non-repeating tasks. Currently, the state-ofthe-art feedforward controller dedicated to suppressing residual vibration in robot arms is time-varying input shaping (TVIP). However, TVIP falls short in trajectory tracking tasks since the method adds delays in the commands creating errors in tracking and thereby contouring trajectories. Therefore, this paper proposes the use of an alternate feedforward method, known as the filtered B-splines (FBS) approach, to suppress vibration in six DOF robots while maintaining tracking accuracy. Since time-varying FBS (TVFBS) requires full frequency response functions (FRFs), compared to only natural frequencies and damping ratios for TVIP, we propose a framework for estimating the FRFs of serial kinematic chain 6-degree-of-freedom robots. Residual vibration reduction experiments and trajectory tracking experiments, in which the dynamics of a UR5e collaborative robot change considerably, were carried out to validate the model prediction framework. TVFBS reduced the end-effector vibration by 87% while improving tracking performance in both the y (22%) and z (29%) directions. On the other hand, TVIP worsened the tracking performance (-683.43%) for the y and -662.37%for the z direction) despite the excellent vibration reduction (98%). Hence, TVFBS demonstrated significantly better tracking performance than TVIP while retaining comparable vibration

Index Terms—Industrial robots, System identification, Timevarying dynamics, Configuration dependent dynamics, Vibration suppression, Feedforward Control, Input shaping, Filtered B-

I. Introduction

Six-degree-of-freedom (DOF) industrial robots are used in a variety of trajectory tracking tasks like additive manufacturing, spray and inkjet painting, and spot and arc welding. Robots have several advantages when performing these tasks, including the dexterity to follow complex 3D paths, repeatability in their operation, and the ability to cover large workspaces. However, these processes are typically very time-consuming

This work was supported by the U.S.National Science Foundation [grant CMMI 2054715]

because the robots are commanded to move at lower speeds when compared to their full capability. A major reason to slow down is the vibrations experienced at the end-effector due to the structural flexibility in the kinematic chain of the robot [1]. Therefore, one can conclude that there is a trade-off between speed and accuracy since vibration errors degrade the accuracy of the tracking task. Eliminating vibration while increasing speed on six DOF robots can be achieved by a number of methods including feedback control, iterative learning control, and feedforward control.

There are two common applications of feedback control in six DOF robots, passivity-based control and feedback control using an external sensor. Passivity-based control requires the full analytical model of the robot, including motor dynamics. flexible-joint dynamics, and link dynamics [2]. Such a model is difficult to obtain for robot users since the robot manufacturers do not share the dynamic parameters of their products or install the necessary sensors to estimate them due to cost constraints. The second method involves using an external sensor to measure the state of the end-effector and applying a control input to the joint actuators to correct tracking errors [3]. This approach results in a system where the sensing and actuation are non-collocated, which can result in stability issues [4]. Additionally, delays from the measurement to the control input may cause additional errors [3].

Iterative learning control (ILC) improves trajectory tracking accuracy by learning the errors from previous executions (i.e., iterations) of a particular trajectory and correcting them in future iterations [5]. As such, it is ideal for systems that execute repetitive tasks, where an ILC model can be trained once and used over again. However, a major limitation of ILC is that the trained controller does not work well for nonrepetitive motions [5].

Feedforward control can be used to overcome the aforementioned weaknesses of feedback control and ILC because it allows robot users to measure the dynamics of the system asis, does not create stability issues, and works for repeating and non-repeating trajectories [6]. Currently, the state-of-the-art feedforward controller to suppress residual vibration in robot arms is time-varying input-shaping. In a recent paper, Newman et al. [7] used data from a theoretical dynamic model of a six DOF robot arm to train a neural network to estimate the natural frequencies and damping ratios of the vibration modes related to the first three joints. The predictions were used to update input shaping producing up to 85% vibration reduction in different poses during their tests. Similarly, Thomsen et al. [8] described a procedure for identifying and mapping the natural frequency and damping ratio of second-order models related to the vibration modes generated by the major flexible joints of a six DOF robot. Using the identified parameters, the authors applied a time-varying input shaping achieving up to 90% vibration mitigation during point-to-point (PTP) moves. Despite the success of both [7] and [8] in reducing vibration in PTP motions, it is well-known that input shaping creates errors in tracking and thereby contouring trajectories in systems with linear stages [9]. This limitation is severe when the same method is used in robots with serial kinematic structures since the end-effector motion is generated by a combination of multiple joint rotations. Hence, the current state-of-the-art feedforward control method to suppress residual vibration in robot arms falls short in trajectory tracking tasks.

This paper proposes the use of an alternate method, known as the filtered B-splines (FBS) approach, to suppress vibration in six DOF robots while maintaining tracking accuracy. FBS has been used to suppress vibration in other tracking applications, including CNC machines [10] and 3D printers [6] resulting in up to 2x increase in the end-effector trajectory speed without sacrificing quality in additive manufacturing. Similar to input shaping, the FBS approach is a model-based feedforward control technique. However, while input shaping requires determining the natural frequency and damping ratio of the vibration modes (i.e., only the poles of a transfer function) [8], FBS uses full frequency response functions (FRFs) (i.e., both poles and zeros of a transfer function) [6], which requires fitting more model parameters.

The time-varying (i.e., pose-dependent) nature of the robot's dynamics intensifies the challenge of obtaining FRFs since the parameters of the poles and zeros must evolve with the robot's pose. Edoimioya et al. [11] proposed a physics model-based framework capable of estimating the FRFs of a delta 3D printer. The parallel kinematic chain of the delta robot allowed the authors to approximate part of the dynamics of the system as time-invariant, simplifying the model estimation. However, this assumption does not hold for time-varying systems with serial kinematic chains such as robot arms.

Therefore, this paper:

- Proposes a framework for measuring and estimating the full FRFs of serial kinematic chain robots for any pose in the workspace using no external hardware to identify the system dynamics, and
- 2) Demonstrates that the filtered B-splines approach can be implemented in robot arms achieving comparable vibration suppression while significantly improving tracking accuracy when compared to the state-of-the-art feedforward controller to reduce residual vibration, time-varying

input shaping.

II. SIMPLIFYING ASSUMPTIONS FOR ESTIMATING ANALYTICAL FRFS

In this work, it is assumed that the mechanical flexibility of the robot can be approximated as an equivalent torsional stiffness at the joints, representing the link and gearbox flexibility. Therefore, the control action of the proposed feedforward controller will focus on three vibration modes: rotations about the base, shoulder, and elbow joints.

There are three main reasons for selecting those vibration modes. First, for most robotic applications, motions in the x, y, and z directions have larger magnitude and speeds than the pitch, yaw, and roll rotations. Therefore, it is reasonable to assume that the vibration modes with respect to the base, shoulder, and elbow joints will primarily be excited. Second, due to the robot's kinematics, small angular displacement on the selected joints can significantly affect the end-effector position. Third, the base, shoulder, and elbow joints experience relatively higher inertia than the wrist joints. Therefore, their corresponding modes will present lower natural frequencies.

The simplified model of the robot can be expressed by

$$\mathbf{M}\ddot{\mathbf{q}} + \mathbf{B}\dot{\mathbf{q}} + \mathbf{K}\mathbf{q} = \mathbf{B}\dot{\mathbf{q}}_d + \mathbf{K}\mathbf{q}_d \tag{1}$$

where **M** is the mass matrix, **K** is the stiffness matrix, **B** is the damping matrix, **q** is the vector of the actual joint angle, and \mathbf{q}_d is the motor angle. Note that the Corriolis and gravitational terms are neglected in this simplified model. More information about the robot model can be found in [7] and [12].

Fortunately, the vibration modes of the base, shoulder, and elbow joints can be partially decoupled. The coupling between the vibration modes occurs due to the presence of non-diagonal terms in the inertia matrix while the stiffness, **K**, and damping matrices, **B**, are diagonal [7]. Here, it is assumed that the shoulder and elbow modes are coupled while the base mode is decoupled because the non-diagonal terms in the first row and column of the inertia matrix are negligible when compared to the base moment of inertia. Based on these assumptions, the above equation can be expressed in the Laplace domain as

$$\mathbf{Q} = (\mathbf{M}s^2 + \mathbf{B}s + \mathbf{K})^{-1} (\mathbf{B}s + \mathbf{K}) \mathbf{Q}_d$$
 (2)

where

$$\mathbf{M} = \begin{bmatrix} m_{11} & 0 & 0 \\ 0 & m_{22} & m_{32} \\ 0 & m_{32} & m_{33} \end{bmatrix}; \mathbf{B} = [b_i]_{3x3}; \mathbf{K} = [k_i]_{3x3}$$

From Eq. 2, the system dynamics can be represented as follows:

$$\underbrace{\begin{bmatrix} Q_{1}(s) \\ Q_{2}(s) \\ Q_{3}(s) \end{bmatrix}}_{\mathbf{Q}} = \begin{bmatrix} G_{11} & 0 & 0 \\ 0 & G_{22} & G_{23} \\ 0 & G_{32} & G_{33} \end{bmatrix}}_{\mathbf{Q}} \underbrace{\begin{bmatrix} Q_{d1}(s) \\ Q_{d2}(s) \\ Q_{d3}(s) \end{bmatrix}}_{\mathbf{Q}_{d}} \tag{3}$$

Using Eq. 3, it is possible to define the transfer function representing the robot's dynamics when the base (G_1) , shoulder (G_2) , or elbow (G_3) joint is used to excite the system. The transfer functions are presented below:

$$G_1 = \frac{\mathcal{L}\{q_1\}}{\mathcal{L}\{q_{d1}\}} = G_{11} = \frac{a_1 s + a_2}{a_3 s^2 + 2a_4 s + a_5}$$
(4)

$$G_2 = \frac{\mathcal{L}\{q_2\}}{\mathcal{L}\{q_{d2}\}} = G_{22} + G_{32} = \frac{d_1s^3 + d_2s^2 + d_3s + d_4}{d_5s^4 + d_6s^3 + d_7s^2 + d_8s + d_9}$$
(5)

$$G_3 = \frac{\mathcal{L}\{q_3\}}{\mathcal{L}\{q_{d3}\}} = G_{33} + G_{23} = \frac{c_1 s^3 + c_2 s^2 + c_3 s + c_4}{c_5 s^4 + c_6 s^3 + c_7 s^2 + c_8 s + c_9}$$
(6)

where a_i , d_i , and c_i are the coefficients of the transfer functions. The actual joint positions, \mathbf{q} , should be measured by a rotary encoder placed after the gearbox of the joint. However, most robots do not have those sensors, therefore, \mathbf{q} will be estimated using the end-effector accelerometer readings. More information about how to estimate the joint's output using accelerometer readings can be found in [8].

III. OVERVIEW OF CONTROL METHODS

A. Time-Varying Filtered B-splines Approach

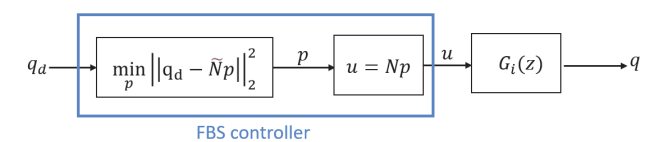


FIGURE 1. Block diagram for tracking control using filtered B-splines (FBS) approach.

Consider a stable linear time-varying discrete-time system, $G_i(z)$, representing an open-loop or close-loop plant with a nonzero DC gain. As shown in Fig. 1, a feedforward tracking controller, C, controls $G_i(z)$ aiming at generating a control trajectory, u(k), resulting in an output trajectory, q(k), sufficiently close to the desired, $q_d(k)$, after the input passes through $G_i(z)$. Note that z is the forward shift operator and $0 \ge k \ge E$, $k \in \mathbb{Z}$ where E+1 is the number of discrete points in the trajectory. In the full-preview filtered B-splines approach [13], q_d is assumed to be entirely known a priori and u is expressed as

$$\mathbf{u} = \begin{bmatrix} N_{0,m}(\xi_0) & N_{1,m}(\xi_0) & \cdots & N_{n,m}(\xi_0) \\ N_{0,m}(\xi_1) & N_{1,m}(\xi_1) & \cdots & N_{n,m}(\xi_1) \\ \vdots & \vdots & \ddots & \vdots \\ N_{0,m}(\xi_E) & N_{1,m}(\xi_E) & \cdots & N_{n,m}(\xi_E) \end{bmatrix} \mathbf{p}$$
(7)

where **N** is the matrix of B-spline basis functions of degree m, **p** is a vector of n+1 unknown coefficients (or control points), j=0, 1,...,n, and $\xi \geq [0,1]$ is the spline parameter,

representing normalized time, which is discretized in Eq. 7 into E+1 uniformly spaced points, $\xi_0, \xi_1, \ldots, \xi_E$. More information about the basis functions can be found in [13].

Similarly to \mathbf{u} , let vectors \mathbf{q}_d and \mathbf{q} represent the E+1 discrete points of q_d and q, respectively. Based on the definition of \mathbf{u} in Eq.7, \mathbf{q} can be described as

$$\mathbf{q} = G_i \mathbf{u} = G_i \mathbf{N} \mathbf{p} = \widetilde{\mathbf{N}} \mathbf{p} \tag{8}$$

where $\hat{\mathbf{N}}$ is the filtered B-splines matrix, acquired by passing each column of $\hat{\mathbf{N}}$ through the dynamic system $G_i(z)$, which changes with the robot's pose [11]. Therefore, each row of the filtered B-spline matrix is a combination of the B-splines and the impulse response of the current dynamics of the system at step k, achieved by using the output side algorithm (OSA) finite impulse response (FIR) filter [14]. Finally, the optimal control points are given by the least-squares solution when the two-norm of the tracking error is minimized [13]

$$\min_{\mathbf{p}} \left(\left(\mathbf{q}_d - \tilde{\mathbf{N}} \mathbf{p} \right)^{\top} \left(\mathbf{q}_d - \tilde{\mathbf{N}} \mathbf{p} \right) \right) \to \mathbf{p} = \left(\tilde{\mathbf{N}}^{\top} \tilde{\mathbf{N}} \right)^{-1} \tilde{\mathbf{N}}^T \mathbf{q}_d \quad (9)$$

B. Time-Varying Input Shaping

Input shaping is a feedforward control method to suppress residual vibration generated by the reference trajectory. The method emanates from earlier work on Posicast (positively forecasting) control [15], which involves breaking a step of a certain magnitude into two smaller steps, one of which is delayed in time. This way, the oscillations introduced by the second impulse cancel out the response of the first one. This paper used a robust version of input shaping known as Zero Vibration and Dervative (ZVD) input shaping [7]. The ZVD shaper can be expressed in the Laplace domain as

$$F_{ZVD}(s) = \frac{1 + 2Ke^{-0.5T_d s} + K^2 e^{-T_d s}}{1 + 2K + K^2}$$
(10)

$$K = e^{\frac{-\zeta(k)\pi}{\sqrt{1-\zeta(k)^2}}}; \quad T_d = \frac{2\pi}{\omega_d}; \quad \omega_d = \omega_n(k)\sqrt{1-\zeta(k)^2}$$
 (11)

where $\zeta(k)$ and $\omega_n(k)$ are the damping ratio and natural frequency of the system at time step k, respectively. Therefore, the F_{ZVD} filter is updated every time step and OSA FIR numerical convolution is used to filter the desired trajectory with the time-varying ZVD shaper. More information concerning the impact of OSA FIR numerical convolution in input shaping can be found in [14].

IV. SYSTEM IDENTIFICATION

A. Experimental Setup

Experiments were performed using a UR5e collaborative robot. The robot was mounted on an inertial table Newport *RS* 1000 and Python scripts were written to command the robot during the experiments using a 500 Hz sampling rate. A 5 kg mass was attached to the end-effector for all experiments. The experimental setup is shown in Fig.2.



FIGURE 2. Experimental setup.

B. System Identification Experiment

The system identification experiment was performed to map the pose-dependent dynamics of the robot. To determine the robot's pose, the position of the end-effector was described using polar coordinates, as depicted in Fig. 3. Using polar coordinates reduces the number of variables to map the position of the end-effector across the workspace from x, y, and z coordinates to radius R and angle V, since the robot is symmetric with respect to the base joint axis [8].

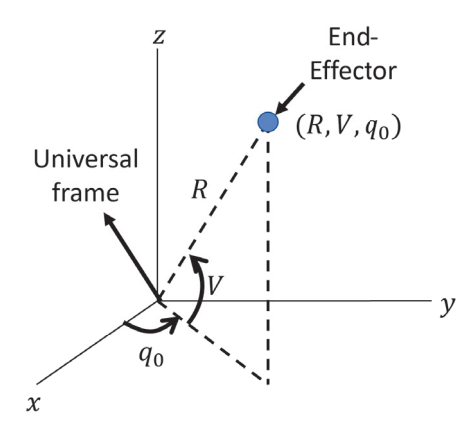


FIGURE 3. Representation of the end-effector poison across the workspace using polar coordinates.

The system identification Python script allowed the experiment to be done autonomously for several poses. For each pose, the robot's structure was excited by sending a sine sweep input to the base, shoulder, and elbow joints, respectively. The sine sweep used a frequency range of 0.5 to 60 Hz with a frequency step of 0.5 Hz and a maximum acceleration of $10 \frac{\text{rad}}{\text{s}^2}$. Although other researchers have used a bang-cost-bang input to experimentally determine the natural frequencies of the robot [14], using a sine sweep produces considerably better experimental FRFs.

The robot dynamics were identified throughout the entire workspace, ranging R from 0.2 m to 0.65 m with a distance step of 0.05 m and V from 0° to 90° with an angular step

of 5°. Therefore, a total of 190 (#poses) x 3 (#joints) = 570 experimental FRFs were collected and their model parameters were extracted following the procedure described in Fig.4. As a result, 20 nonlinear models were generated to estimate the system dynamics in any region of the workspace.

From the identified models, the poles and zeros of all transfer functions are extracted. By using the corresponding robot pose, a nonlinear model can be established between the endeffector position and all the transfer function parameters by solving a nonlinear least squares problem via the Levenberg-Marquardt algorithm [17]. As a result, each parameter of the transfer functions will have a nonlinear model in which R and V are the inputs of the model and ω_n or ζ are the outputs. The system identification process is summarized in Fig. 4.

V. EXPERIMENTAL COMPARISON BETWEEN TVFBS AND TVIP

Two experiments were performed to evaluate the performance of time-varying FBS. The end-effector trajectories of both experiments were generated using a trapezoidal velocity profile considering 580 $\frac{mm}{s}$ and 9000 $\frac{mm}{s^2}$ as maximum velocity and acceleration, respectively. The time-varying dynamics for both experiments are shown in Table I.

TABLE I. Changes of the natural frequencies of the system for the residual vibration reduction and trajectory tracking experiment.

System Dynamics	1 st pole (Hz)	2 nd pole (Hz)
G_2	9 – 17	24 - 31
G_3	9 - 16	25 - 30

A. Model Generation

Once the nonlinear models are determined from the system identification experiment, it is possible to estimate the system dynamics given q_0 and the end-effector Cartesian trajectory by calculating R and V. The model estimation framework used in both performance evaluation experiments is summarized in Fig. 5.

It was observed that only the parameters of the complex conjugate poles and zeros demonstrate a strong correlation with the robot's pose which was expected since they represent the mechanical resonance and anti-resonance of the system, respectively. Therefore, the system dynamics can be approximated by

$$G_{i} \approx kG_{m_{i}} \rightarrow \begin{cases} G_{m_{2}}, G_{m_{3}} = \frac{(s-z_{1})(s-z_{1}^{*})}{(s-p_{1})(s-p_{1}^{*})(s-p_{2})(s-p_{2}^{*})} \\ G_{m_{1}} = \frac{1}{(s-p_{1})(s-p_{1}^{*})} \end{cases}$$
(12)

where $k = \frac{1}{G_{m_i}(0 \text{Hz})}$, z_i and z_i^* are the complex conjugate zeros, and p_i and p_i^* are the complex conjugate poles, which can be estimated using nonlinear models (Fig. 4).

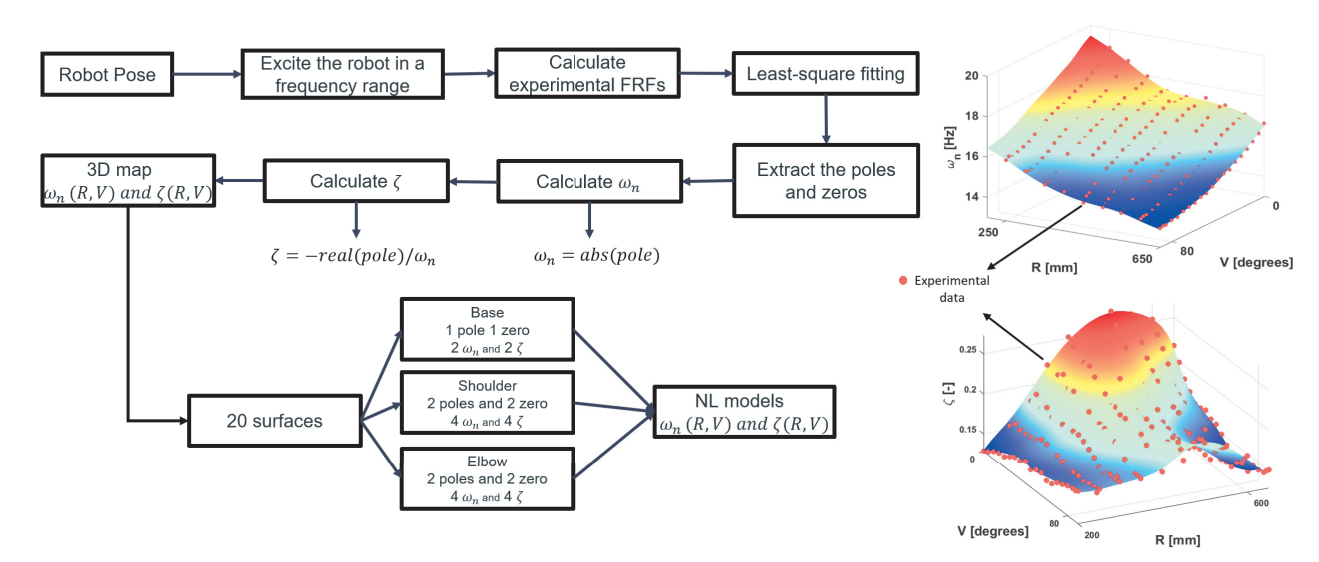


FIGURE 4. System Identification procedure to map the pose-dependent dynamics of the robot. The natural frequency and damping ratio 3D maps and nonlinear models of one pole of G_2 are presented.

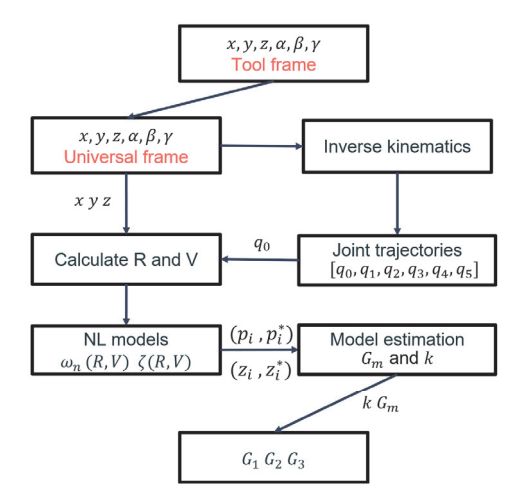


FIGURE 5. Model estimation framework. α is the pitch angle, β is the yaw angle, γ is the row angle, (p_i, p_i^*) are complex conjugate poles, (z_i, z_i^*) are the complete conjugate zeros, and k is the correction of the DC gain.

B. Residual Vibration Experiment

In this experiment, the residual vibration performance of time-varying FBS (TVFBS) and time-varying input-shaping (TVIP) are compared. The robot is commanded to perform a point-to-point motion in which the end-effector goes from one extreme region of the workspace to another, changing the system dynamics considerably as depicted in Table I and Fig.6.

To analyze the residual vibration, the end-effector acceleration is measured after the end of the motion using the UR5e's built-in accelerometer, and the vibration reduction is presented in both frequency and time domains. For the frequency domain analysis, the vibration energy is analyzed [8].

The experimental results for the residual vibration reduction experiment are presented in Figs. 7 and 8. The results indicate

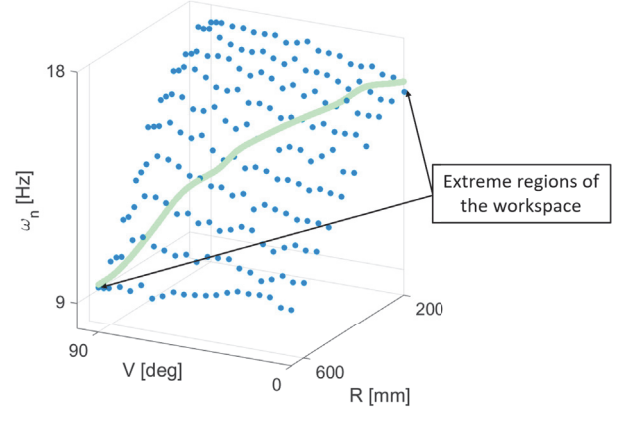


FIGURE 6. 3D map of the one natural frequency of G_3 . Line [—] describes the changes of the one ω_n for the point-to-point motion.

that TVIP presented a better vibration reduction (98.20%) than TVFBS (87.55%). The percentages were calculated based on the frequency domain analysis (Fig. 8).

Contrasting the TVFBS and TVIP, both controllers presented comparable performances although input shaping showed superior vibration reduction, which was expected since input shaping was developed to suppress residual vibration. On the other hand, FBS was primarily developed to improve the trajectory tracking performance of a system given its dynamics. In other words, the vibration reduction produced by FBS is an effect of the improvements made in trajectory tracking.

Finally, it should be highlighted that both controllers presented considerable vibration reduction, indicating that the framework for estimating the robot's dynamics yields satisfactory model prediction.

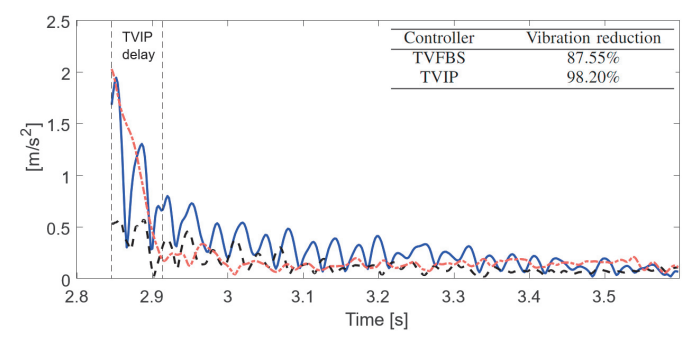


FIGURE 7. Acceleration norm of the accelerometer readings showing the residual vibration in the time domain. TVFBS [——]; TVIP [——]; Baseline [——]

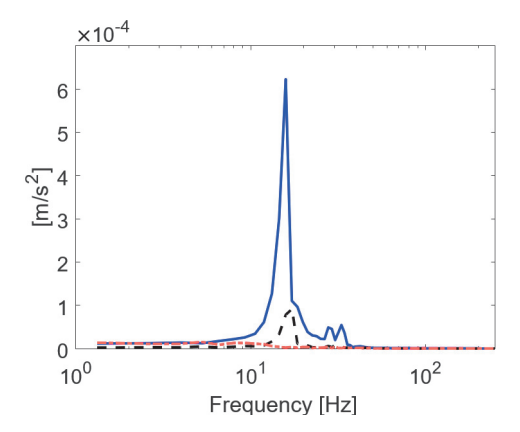


FIGURE 8. Frequency domain analysis of the residual vibration. TVFBS [——]; TVIP [——]; Baseline [——]

C. Trajectory Tracking Experiment

In this experiment, the tracking performance of TVFBS and TVIP are compared. The robot is commanded to perform a gear shape motion in which the end-effector goes from one extreme region of the workspace to another changing the system dynamics considerably, as depicted in Table I.

To analyze the improvements in tracking performance, the root-mean-square (RMS) of the end-effector tracking error was calculated with respect to the baseline. The end-effector position was estimated using a Luenberger observer with a bandwidth of 10 Hz, in which the low-frequency components mostly rely on the estimated models while the high-frequency components predominantly depend on the acceleration measurements. It should be mentioned that the same observer was used to calculate the end-effector position in all experiments, meaning any bias/uncertainty related to the observer estimation did not affect the comparison of the controllers' performance.

The experimental results for the trajectory tracking experiment are presented in Fig. 9. The results indicate that TVFBS improves the end-effector tracking performance in both the *y* (22.49%) and *z* (29.384%) directions. When both feedforward controllers are compared, TVFBS presented considerably better tracking performance than TVIP (-683.43% for the *y* and -662.37% for the *z* direction), as depicted in Fig. 9(a) and

(b). This result was expected since the considerable vibration reduction of input shaping comes with the trade-off of creating delays in the commands, generating great contour errors at the end-effector trajectory as shown in Fig. 10.

VI. CONCLUSIONS

This paper presents a framework for estimating the frequency response function (FRFs) of robotic arms. Work from [7] and [8] proposed model estimation frameworks that predict the natural frequency and damping of the vibration modes related to the first three or two joints of an industrial robot, respectively. On the other hand, [11] presents a framework that can estimate the full FRFs of parallel kinematic chain robots but model assumptions made for parallel robots do not hold for robotic arms. Therefore, this paper proposes a framework that is able to estimate the full FRFs of serial kinematic manipulators accurately. The models generated enabled the use of the feedforward tracking controller, the so-called time-varying filtered B-splines (TVFBS) approach, in a six DOF industrial robot. The method was validated based on an experimental implementation in a UR5e collaborative robot.

A residual vibration reduction experiment showed that TVFBS and TVIP presented comparable performances although input shaping demonstrated superior vibration reduction. Hence, one can conclude that a framework for estimating the robot's dynamics yields satisfactory model prediction. Additionally, a trajectory-tracking experiment demonstrated that TVFBS presented considerably better tracking performance while maintaining comparable vibration reduction to TVIP. This result demonstrates that TVFBS can provide superior performance in tracking applications when compared to the state-of-the-art feedforward controller to reduce vibration in robot arms.

Future work that builds on this paper include the following:
1) proposing an intelligent way of reducing the number of poses in the system identification experiment without compromising prediction quality; 2) implementing the real-time version of FBS; and 3) proposing a general system identification procedure to experimentally identify the vibration modes of the end-effector regardless of the robot dynamics.

ACKNOWLEDGMENT

The authors would like to acknowledge the U.S.National Science Foundation that supported this work through the grant CMMI 2054715.

REFERENCES

- Bhatt, P.M., Malhan, R., Shembekar, A.V., Yoon, Y.J. and Gupta, S.K., "Expanding capabilities of additive manufacturing through use of robotic technologies: a survey," *Additive Manufacturing*, vol. 31, 100933, 2020, doi: 10.1016/j.addma.2019.100933.
- [2] Albu-Schaffer, A., Ott, C., and Hirzinger, G. "A unified passivity-based control framework for position torque impedance control of flexible joint robots," *International Journal of Robotics Research*, vol. 26, no. 1, pp. 23–39, 2007, doi: 10.1177/02783649070737.
- [3] Woodside, M.R., Fischer, J., Bazzoli, P., Bristow, D.A., and Landers, R.G. "A Kinematic Error Controller for Real-Time Kinematic Error Correction of Industrial Robots," *Procedia Manufacturing*, vol. 53, pp. 705–715, 2021, doi: 10.1016/j.promfg.2021.06.069.

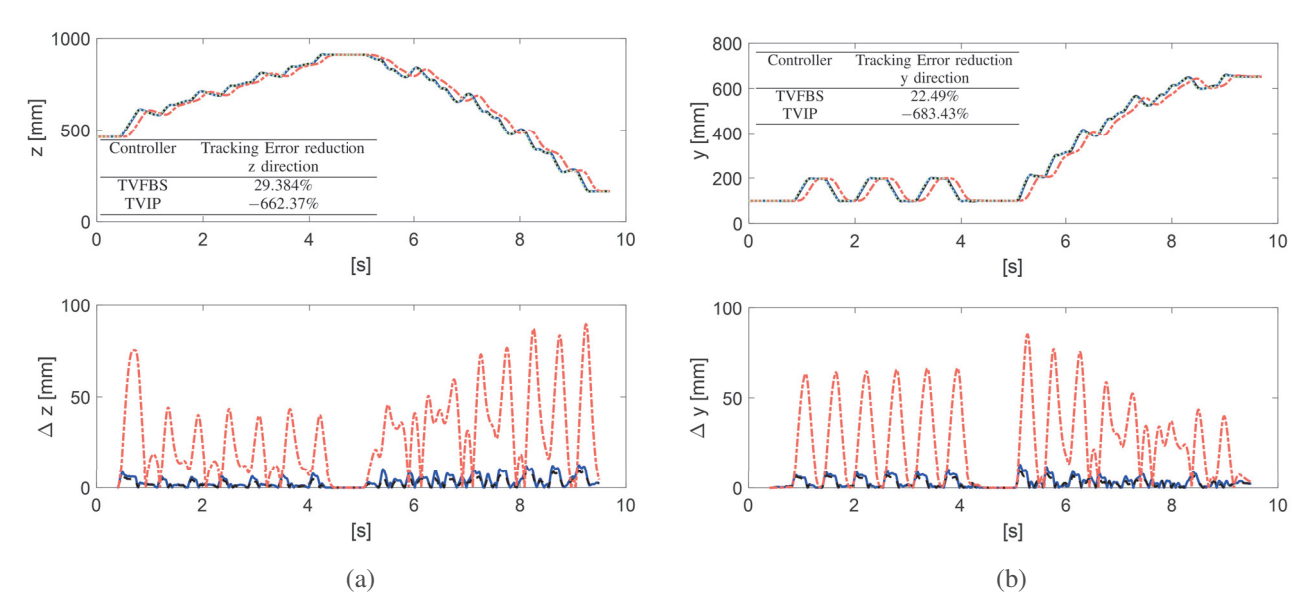


FIGURE 9. Gear shape trajectory of the end-effector estimated by the Luenberger observer. (a) z direction and its tracking error Δ z; (b) y direction and its tracking error Δ y. Reference [——]; TVFBS [——]; TVIP [——]; Baseline [——]

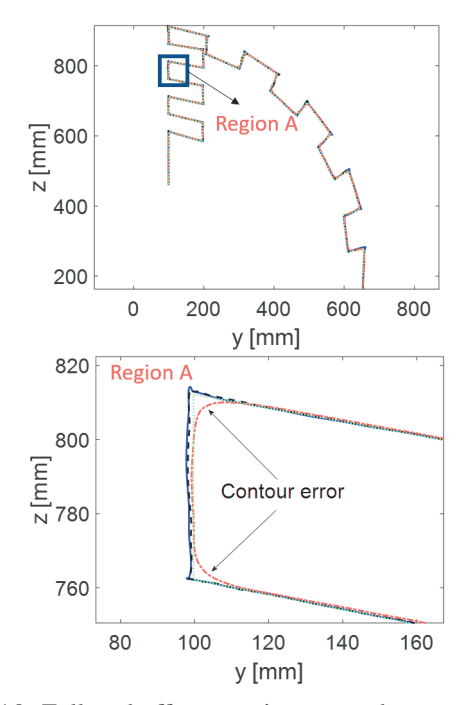


FIGURE 10. Full end-effector trajectory and contour error in detail. TVFBS [——]; TVIP [——]; Baseline [——]

- [4] Miu, D., Mechatronics, Springer-Verlag, New York, 1993.
- [5] Bristow, D.A., Tharayil, M., and Alleyne, A.G., "A survey of iterative learning control," *IEEE Control Systems Magazine*, vol. 26, no. 3, pp. 96-114, 2006, doi: 10.1109/MCS.2006.1636313.
- [6] Duan, M., Yoon, D., and Okwudire, C.E., "A limited-preview filtered B-spline approach to tracking control – with application to vibrationinduced error compensation of a 3D printer," *Mechatronics* vol. 56, pp. 287-296, 2018, doi: 10.1016/j.mechatronics.2017.09.002.

- [7] Newman, M., Lu, K. and Khoshdarregi, M., "Suppression of robot vibrations using input shaping and learning-based structural models," *Journal of Intelligent Material Systems and Structures*, vol. 32, no. 9, pp. 1001-1012, 2021, doi: 10.1177/1045389X20947166.
- [8] Thomsen, D.K., Soe-Knudsen, R., Balling, O., and Zhang, X., "Vibration control of industrial robot arms by multi-mode time-varying input shaping," *Mechanism and Machine Theory*, vol. 155, 104072, 2021, doi: 10.1016/j.mechmachtheory.2020.104072.
- [9] Singhose, W. and Singer, N. "Initial investigations into the effects of input shaping on trajectory following," *Proceedings of 1994 American Control Conference* vol. 3, pp. 2526–2532, June 1994, doi: 10.1109/ACC.1994.735014.
- [10] Kim, H. and Okwudire, C.E. "Intelligent feedrate optimization using a physics-based and data-driven digital twin," In *CIRP Annals Manufacturing Technology*, vol. 72, no. 1, pp. 325–328, 2023, doi: 10.1016/j.cirp.2023.04.063.
- [11] Edoimioya, N., Chou, C.-H., and Okwudire, C.E. "Vibration compensation of delta 3D printer with position-varying dynamics using filtered Bsplines," *International Journal of Advanced Manufacturing Technology*, vol. 125, pp. 2851–2868, 2023, doi: 10.1007/s00170-022-10789-w.
- [12] Kebria, P.M., Al-Wais, S., Abdi, H., and Nahavandi, S., "Kinematic and dynamic modelling of UR5 manipulator," In 2016 IEEE international conference on systems, man, and cybernetics (SMC), pp. 004229-004234, 2016, doi: 10.1109/SMC.2016.7844896.
- [13] Duan, M., Ramani, K.S., and Okwudire, C.E., "Tracking control of non-minimum phase systems using filtered basis functions: a NURBS-based approach," ASME Dynamic Systems and Control Conference, vol. 57243, V001T03A006, 2015, doi: 10.1115/DSCC2015-9859.
- [14] Thomsen, D.K., Søe-Knudsen, R., Brandt, D., Balling, O., and Zhang, X., "Smooth online time-varying input shaping with fractional delay FIR filtering," *Control Engineering Practice*, vol. 88, pp. 21-37, 2019, doi: 10.1016/j.conengprac.2019.04.003.
- [15] Smith, O. and Mitchell, J., "Feedback control systems," McGraw-Hill, New York, p. 338, 1958.
- [16] Singh, T., and Singhose, W., "Input shaping/time delay control of maneuvering flexible structures," *Proceedings of the 2002 American Control Conference*, vol. 3. 2002. doi: 10.1109/ACC.2002.1023813.
- [17] Gavin, H.P. "The Levenberg-Marquardt algorithm for nonlinear least squares curve-fitting problems," Department of Civil and Environmental Engineering, Duke University, 2019.